Adsorption of Atomic Oxygen and Nitrogen at β-Cristobalite (100): A Density Functional Theory Study

C. Arasa, P. Gamallo, and R. Sayós*

Departament de Química Física i Centre de Recerca en Química Teòrica, Universitat de Barcelona, C. Martí i Franquès 1, 08028 Barcelona, Spain

Received: December 31, 2004; In Final Form: May 3, 2005

The adsorption of atomic oxygen and nitrogen on the β-cristobalite (100) surface is investigated from first principles density functional calculations within the generalized gradient approximation. A periodic SiO_2 slab model (6 layers relaxing 4 or 6) ended with a layer of Si or O atoms is employed throughout the study. Several adsorption minima and diffusion transition states have been characterized for the two lowest spin states of both systems. A strong chemisorption is found for either O or N in several sites with both slab endings (e.g., it is found an average adsorption energy of 5.89 eV for O (singlet state) and 4.12 eV for N (doublet state) over the Si face). The approach of O or N on top O gives place to the O_2 and NO abstraction reactions without energy barriers. Atomic sticking coefficients and desorption rate constants have been estimated (300−1900 K) by using the standard transition state theory. The high adsorption energies found for O and N over silica point out that the atomic recombination processes (i.e., Eley−Rideal and Langmuir−Hinshelwood mechanisms) will play a more important role in the atomic detachment processes than the thermal desorption processes. Furthermore, the different behavior observed for the O and N thermal desorption processes suggests that the published kinetic models for atomic O and N recombination reactions on SiO_2 surfaces, based on low adsorption energies (e.g., 3.5 eV for both O and N), should probably be revised.

1. Introduction

Modeling of the different heterogeneous processes involved in nonequilibrium vibrational kinetics of air hitting over silicon dioxide surfaces is necessary for the study and the design of new thermal protection systems (TPS) to be used in atmospheric terrestrial reentry vehicles.[1] TPS coatings for space vehicles must have very low catalytic efficiency to reduce the surface heat flux due to atomic recombination effects.

Forthcoming development of reusable launch vehicles (RLV) is a prerequisite for guaranteeing long-term access to space. New materials that allow the reduction of launch mass, improved modeling of aerothermodynamic phenomena, increased performance and reliability of propulsion systems, and innovative TPS are required to fulfill RLV objectives. The mastering of the detailed chemical physics phenomena associated with TPS catalysis is therefore a key element in this context. Therefore, theoretical, numerical, and experimental developments are necessary in order to model more accurately the corresponding gas−surface interactions.

Currently, silica-based materials (e.g., reaction-cured glass (RCG) with 94% of SiO_2, 4% of B_2O_3, and 2% of SiB_4) are primarily used in TPS surfaces, where catalytic atomic recombination of oxygen and nitrogen (via Eley−Rideal (ER) or Langmuir−Hinshelwood (LH) mechanisms) plays an important role in reentry heating at thermal nonequilibrium conditions. However, other elementary processes need to be also included in the global kinetic modeling in these conditions:[1,2] atomic adsorption−desorption, molecular adsorption−desorption, atom−molecule ER or LH reactions, etc. Among the different elementary steps involved in the heterogeneous catalysis—(1) diffusion of reactants to the surface, (2) adsorption of reactants on surface, (3) chemical reactions on surface, (4) desorption of products from surface, and (5) diffusion of products away from the surface—steps 1 and 5 are usually fast, and the rate-determining step has to be found among steps 2, 3, and 4.

The main goal of our research in progress is the theoretical study from first principles of the steps 2, 3, and 4 with several models of a silica surface in order to provide kinetic and dynamical data useful for computational fluid dynamics (CFD) simulations. Published kinetic models for air recombination over SiO_2-based materials incorporate rough estimates of several important physiochemical quantities (sometimes used as adjustable parameters), such as, for example, atomic adsorption energies, atomic sticking coefficients, the number of adsorption sites by unit area, and others. We believe that a deep theoretical understanding on these processes will permit the proposal of new less catalytic materials to be used as TPSs.

In a first step of the work we have to study the O and N adsorption processes. Nevertheless, scarce experimental data are available on both processes, which are usually treated in a similar way by means of an average adsorption energy of 3.5 eV[1] regardless of the kind of silica surface (e.g., Pyrex, quartz, RCG, etc.), although several used values are within the range of 2.6−5.5 eV.[2−6] These data are indirectly derived from kinetic modeling of atomic recombination on SiO_2 surfaces to fit some experimental data. Thus, for instance, initial surface sticking coefficients S_0 of $0.05e^{-0.002T}$ (on SiO_2) or $1.0e^{-0.002T}$ (on RCG) and an adsorption energy of 3.5 eV were reported for oxygen in both surfaces;[1] for nitrogen on RCG the reported data were $S_0 = 0.95e^{-0.002T}$ and an adsorption energy of 3.4 eV.[1]

Among the different forms of silicon dioxide to be studied, either amorphous or crystalline (e.g., quartz, tridymite, cristobalite, etc.), the β-cristobalite is the most stable polymorph at

* Author for correspondence. E-mail: r.sayos@ub.edu.

10.1021/jp044064y CCC: $30.25
Published on Web 07/16/2005

high temperatures up to the melting point of 1983 K; these elevated temperatures are achieved during the earth's atmospheric reentry phase. Moreover, β-cristobalite is the crystalline phase of silica with properties closest to those of amorphous silica (e.g., density, refractive index, band structure, etc.). Recent experimental measurements[7,8] of the oxygen recombination coefficient γ_O over silica have shown that this coefficient is 4 times higher for β-cristobalite than for quartz. Another related theoretical work[9] has also studied the kinetics and dynamics of the atomic oxygen recombination (ER and LH mechanisms) over β-cristobalite. They used a semiempirical interaction potential for oxygen on β-cristobalite along with a semiclassical collisional model, which allows to ascertain the importance of both mechanisms depending on the surface temperature. This potential energy surface, as the authors recognize, seems a crude approximation to the real interaction forces, although theoretical and experimental γ values are in reasonable agreement.

In this paper we present a wide theoretical study based on periodic density functional theory (DFT) calculations for the O and N adsorption at β-cristobalite (100), with either O or Si as a first layer. We have considered dehydroxylated β-cristobalite as a first approximation to the real amorphous TPS materials used at high temperatures to simplify the theoretical study and to facilitate its comparison with previous and related theoretical[9] and experimental studies,[7,8] which used α-quartz or β-cristobalite. For instance, the experimental results for γ_O over RCG are quite similar as for α-quartz.[8] Up to our knowledge, this is the first attempt to quantify from first principles these elementary processes, and it is a first stage in the construction of the ab initio potential energy surfaces needed to study the dynamics of the O and N recombination processes over β-cristobalite surfaces (i.e., $O + O_{ad}$, $N + N_{ad}$, $O + N_{ad}$, $N + O_{ad}$, etc.).

2. Computational Method

We have performed DFT calculations by means of the VASP code,[10−13] which uses plane wave basis set. The calculations are based on the generalized gradient correction (GGA) functional Perdew−Wang 91 (PW91).[14,15] The electron−ion interactions were described by using the projector-augmented-wave (PAW) technique,[16,17] particularly good for transition metals and oxides and giving similar results as the FLAPW all-electron method. We checked widely the appropriate energy cutoff in several bulk and slab calculations. Thus, our previous bulk calculations to obtain several properties (e.g., bulk modulus, cell lattice parameters, cohesive energy, etc.) of some silica polymorphs (e.g., α-quartz, β-quartz, β-trydimite, or β-cristobalite) showed that an energy cutoff of 400 eV was accurate enough to obtain converged properties. We have also confirmed this value with some extra slab calculations.

Spin-polarized calculations were carried out to check the ground electronic state of the total system, as both atomic adsorbates (i.e., $O(^3P)$ and $N(^4S)$) are open-shell systems. Integration over the Brillouin zone was performed by using a $3 \times 3 \times 1$ (in slab calculations) or $9 \times 9 \times 9$ (in bulk calculations) k-points mesh by means of the Monkhorst−Pack method.[18] Geometrical optimizations and vibrational frequencies were computed with an energy accuracy of 10^{-6} eV.

For adsorption studies we use a 1×1 surface unit cell and several slab models (4, 6, or 8 layers of SiO_2) for the β-cristobalite (100) face with either an oxygen or a silicon first layer. An additional hydrogen back layer was added to saturate the Si or O dangling bonds as is commonly accepted for silica and silica-containing oxides.[19−21] Thus, to ensure this behavior, the two last layers were always kept fixed while the others were fully or partially relaxed depending on the slab model used. The distance between slabs (ca. $z = 17-18$ Å) was large enough to prevent significant interactions between them.

Despite the large lattice parameter of β-cristobalite, we have also carried out some supplementary adsorption calculations with a 2×2 supercell to check that the atomic coverage effect was very small in the calculated properties.

Several adsorption sites were characterized for O and N adatoms (see next section for details). Once determined the optimal geometry for each adsorption site, we calculated the Hessian matrix and its corresponding harmonic vibrational frequencies (ν_i) for the adatom (i.e., these can be approximately classified as two parallel and one perpendicular movements), keeping fixed the optimized slab geometry. Several calculations introducing a slab relaxation (i.e., 2 or 4 layers) were carried out to verify that the vibrational frequencies were essentially the same. This analysis allowed the complete characterization of minima (i.e., 3 real ν_i) and surface diffusion transition states (i.e., 1 imaginary frequency (first-order saddle point) or 2 imaginary frequency ($2n$-order saddle point)).

The adsorption energy (E_{ad}) was defined as

$$E_{ad} = E(\text{atom}) + E(\text{slab}) - E(\text{atom} + \text{slab}) \qquad (1)$$

where E(atom) is the total calculated ground-state energy of the atom in gas phase (i.e., $O(^3P)$ or $N(^4S)$), E(slab) is the value for the relaxed clean slab in its singlet state, and E(atom + slab) is the value of the full relaxed slab containing the adatom. Therefore, when we report a positive adsorption energy for a particular site (e.g., in tables), it means that this site is a minimum (stationary point), which is more stable than the atom + slab asymptote; on the contrary, a negative adsorption energy corresponds to another stationary point (usually a transition state) less stable than the atom + slab asymptote. Thus, minima should be considered as the true adsorption sites.

The atomic energies were calculated with the atom inside large broken symmetry boxes (i.e., $8 \times 7.5 \times 7.6$ Å^3); we used some higher boxes (e.g., $16 \times 16.5 \times 16.6$ Å^3) to be sure that we obtain the same converged energies. Despite the well-known problem about the uncertainty in the DFT energy of systems with a degenerate ground state (e.g., B, N, or O atoms) owing to the usual density functionals for the exchange-correlation energy are not invariant over the set of ground-state densities,[22] the small uncertainty (0.1−0.2 eV for second and third period group elements[23]) compared with the large adsorption energies makes sure that the main conclusions of the present study will be unaltered. Moreover, this uncertainty is lower than or similar to the differences that can be derived from the use of other functionals (e.g., Perdew−Burke−Ernzerhof (PBE)[24]); thus, for instance, our calculated dissociation energies (D_e) of N_2 and O_2 molecules in gas phase were 0.23 and 0.22 eV lower for the PBE than for the PW91 functional, respectively. A recent study comparing the chemisoption energetics of atoms and molecules on transition-metal surfaces[25] with different GGA functionals (i.e., PW91, PBE, revPBE, and RPBE) reveals that for O, CO, and NO over Ni, Rh, and Pd (with several faces and sites) the maximum average difference between calculated chemisorption energies with different functionals is ~0.5 eV, and the maximum average difference between calculated and experimental values is about 0.6 eV.

3. Results and Discussion

3.1. Bulk and Slab Calculations for the β-Cristobalite. β-Cristobalite is formed by extended layers with SiO_4 tetrahedral

TABLE 1: Calculated and Experimental Properties for the Bulk Structure of β-Cristobalite

	DFT-GGA/PW91			experimental		
	*Fd*3*m* (ideal fcc)	$I\bar{4}2d$ (tetragonal)	$P2_13$ (sc)	*Fd*3*m*[a] (ideal fcc)	$I\bar{4}2d$[b](tetragonal)	$P2_13$[a](sc)
$a = b$(Å)	7.453	5.022	7.198	7.159	5.042	7.159
c (Å)	7.453	7.250	7.198	7.159	7.131	7.159
d_{SiO} (Å)	1.614	1.613	1.621	1.550	1.611	1.612
			1.617			1.609
			1.658			1.649
			1.673			1.664
∠SiOSi (deg)	180	147.5	137.2	180	146.7	137.2
			180			180
∠OSiO (deg)	109.5	108.4	101.3	109.5	107.8	101.3
		111.6	116.7		112.8	116.7
			119.1			119.2
			101.3			95.1
E_0[c] (eV/SiO_2)	19.66	19.25	17.77	19.22[d]	19.22[d]	19.22[d]

[a] Reference 26 at 290° C. [b] Reference 28 at 300° C. An orthorhombic (*Fdd*2) unit cell with $a = b = c = 7.131$ Å can also reproduce this polymorph but using 8 instead of 4 SiO_2 units. [c] Cohesive energy derived by using the Murnaghan state equation. [d] Data derived from $\Delta H°$ at 25 °C [32] for the process: SiO_2(β-cristobalite) → Si(g,ideal) + 2O(g,ideal). The experimental value does not distinguish among the three SiO_2 polymorphs (i.e., ideal face-centered cubic, tetragonal, or simple cubic).

units with a 4-fold-coordinated Si at the center and 2-fold-coordinated O atoms at the corners, although some controversial remains about its most stable crystal structure. Thus, ordered cubic structures (*Fd*3*m* and $P2_13$)[26,27] as well as a disordered model (formed by small domains of $I\bar{4}2d$ symmetry distributed in six orientations) with an average pseudocubic *Fd*3*m* structure[28,29] have been experimentally proposed. Recent bulk DFT (LDA and GGA) calculations[30] have been carried out for β-cristobalite using a cubic cell containing eight SiO_2 units with *Fd*3*m* and $P2_13$ spatial symmetries, although a smaller cell with four SiO_2 units would be enough to reproduce *Fd*3*m* (cubic) and $I\bar{4}2d$ (tetragonal) structures. In this study the authors concluded that these structures were energetically almost degenerate over a wide interval of densities. A previous DFT study[31] supports that the pseudocubic structure is the most stable ($F\bar{4}d2$ (or $I\bar{4}2d$) < *Fd*3*m* < $P2_13$) even though the energy difference for the two first is very small (i.e., ∼0.05 eV). Moreover, they considered a bigger unit cell ($F\bar{4}d2$) instead of the equivalent $I\bar{4}2d$ one.

We have also studied the properties of these structures to check the reliability of the present DFT method to reproduce β-cristobalite in bulk and slab models. Thus, Table 1 presents the calculated internal parameters and the cohesive energy of these bulk structures in comparison with available experimental data for the ordered structures. The calculated structural parameters compare well with earlier DFT results[30,31] and with experimental data. The major discrepancy is observed for d_{SiO} in the *Fd*3*m* symmetry, where the calculated value is somewhat higher (i.e., 0.064 Å) than the experimental one. With respect to the energy stability, we found that $P2_13$ is the less stable structure, in agreement with some preceding results,[31] although on the contrary we find that *Fd*3*m* is a bit more stable that the $I\bar{4}2d$ structure. Nevertheless, the differences are within the expected error of the present DFT method, as it was previously discussed in section II (e.g., due to the O atom energy). In addition, we have performed a *Fd*3*m* structure optimization using the PBE functional obtaining that the structural parameters (e.g., $a = b = c = 7.461$ Å, $d_{SiO} = 1.615$ Å, etc.) are in close agreement with those obtained with the PW91 functional, though the cohesive energy decreases in ∼0.5 eV (i.e., $E_0 = 19.11$ eV/SiO_2 molecule), approaching more the experimental value. In general, silica polymorphs (α- and β-quartz, α- and β-cristobalite, β-trydimite, stishovite, etc.) present theoretical (and experimental) cohesive energies very close each other (i.e., <0.1 eV in DFT studies[30−33]), which illustrates the difficulty of the standard DFT methods to be accurate enough to achieve unambiguous conclusions for silica polymorphs.

We have made several slab calculations on singlet state β-cristobalite (100) using 4, 6, or 8 layers (full relaxed arising from the initial *Fd*3*m* bulk geometry) of silica compared with bulk results and to see the validity of the slab model. The results show essentially the same internal parameters for the three models. Thus, we have obtained the following global maximum intervals for the slab structural parameters: $d_{SiO} = 1.612-1.650$ Å, ∠SiOSi = 176.3−179.1°, and ∠OSiO = 108.1−111.2°. These values would match bulk properties between the *Fd*3*m* and the *I*42*d* structures. Interlayer relaxation (i.e., Δd_{12}, Δd_{23}, etc.) analysis shows a significant outward relaxation of the surface plane (∼9.3%) together with smaller inward (∼−1.2%) or outward relaxations (∼1.8%) of the lower layers that partially compensate themselves. Concerning the slab thickness dependence, results for the six-layer slab are well converged within 0.3% (0.007 Å) for the interlayer relaxation, within 0.8% (0.01 Å) for the interatomic distances and 0.7% (0.7°) for the angles.

We have also studied the lowest triplet state to confirm that singlet state was the ground state in the different slab models. Thus, the calculated excitation energies (i.e., singlet−triplet splitting energy defined as $E_{exc} = E_{triplet} - E_{singlet}$) for fixed structures involving 4, 6, or 8 layers were 2.97, 2.99, and 3.01 eV, respectively, compared with 6.42 eV for the bulk calculation. These results corroborate that the singlet state is the ground state for silica. On the other hand, it is observed that the slab models underestimate this energy splitting. This fact agrees with the conclusions derived in an earlier study[34] on self-trapped excitons in α-quartz, which were triplet excited states that distort the crystal locally. The authors concluded that the PW91 functional underestimates the S−T splitting in cases where the triplet state is delocalized, as would correspond to our calculation.

3.2 Atomic Oxygen Adsorption on β-Cristobalite. First, we have studied the atomic oxygen adsorption on the ideal β-cristobalite (100) surface, with a first layer formed by Si atoms. Four different sites have been considered: on top Si (T1), a hollow (H), and two bridges (B1 and B2), as shown in Figure 1. Table 2 presents the results for the atomic adsorption on top Si (site T1) as a function on the slab size. It is observed that the results are almost identical regardless of the number of layers of the slab model, which is consistent with the results about the β-cristobalite models shown in the previous section. Thus, $Si-O_{ad}$ distances are within 0.001 Å, excitation energies within

TABLE 2: Calculated DFT-GGA/PW91 Adsorption Energies, Excitation Energies, and Geometries for Atomic Oxygen on Top Si for the β-Cristobalite (100)−Si-Terminated Surface as a Function of Slab Thickness

layers[a]	spin[b]	E_{exc}(eV)[c]	E_{ad} (eV)[d]	$d_{O_{ad}-Si}$ (Å)[e]
4	0	0	6.00	1.528
		(0)	(6.01)	(1.524)
	1	2.80	3.20	1.525
		(2.79)	(3.23)	(1.528)
6	0	0	6.03	1.528
		(0)	(5.97)	(1.527)
	1	2.81	3.22	1.527
		(2.81)	(3.22)	(1.525)
8	0	0	6.04	1.529
		(0)	(6.05)	(1.523)
	1	2.81	3.23	1.526
		(2.82)	(3.23)	(1.527)

[a] Number of layers of the slab model (apart from the H bottom layer) with a full relaxed structure. Between parentheses are also presented the values for a 2- or 4-relaxed slab model. [b] Total spin quantum number S; $2S+1$ is the electronic state multiplicity. [c] Excitation energy between the two lowest spin states (i.e., singlet an triplet) of the system. [d] Adsorption energy defined in eq 1, without zero point energy corrections. [e] Distance between O adatom and the closest Si atom.

0.03 eV, and adsorption energies within 0.01 eV for full relaxed structures in models with 6−8 layers. This means that the errors due to finite slab thickness will probably not be relevant. Hence, we have finally chosen the six-layer slab model (relaxing the first four layers) to be used in the rest of the work, except in one case shown later.

Table 3 summarizes the results for the four sites. Two strong chemisorptions are found for T1 and B1 sites. In both cases, singlet and triplet states give place to large adsorption energies. Moreover, the singlet state is much more stable than the triplet state in T1 site, whereas a slight opposite behavior is found in B1 site, though with much closer energies in this latter case. This change on the ground spin-state of the system depending on the adsorption site has been also reported for atomic oxygen adsorption over oxides (e.g., MgO(001)[35]), metals (e.g., Pt-(111)[36]), or alloys (e.g., Pt/Ni(111)[37]).

T1 and B1 structures are truly minima as we have verified by the analysis of harmonic vibrational frequencies (Table 3). The different values observed for their vibrational frequencies show the different curvatures of the potential energy surface at these geometries and can be explained analyzing the position of the adatom in each site and its interactions when the adatom is vibrating along the corresponding normal mode. Thus, for O adsorption on T1 site it is observed that the perpendicular frequency is much higher than the two parallel ones (Table 3), whereas on the B1 site the perpendicular is lower than one of

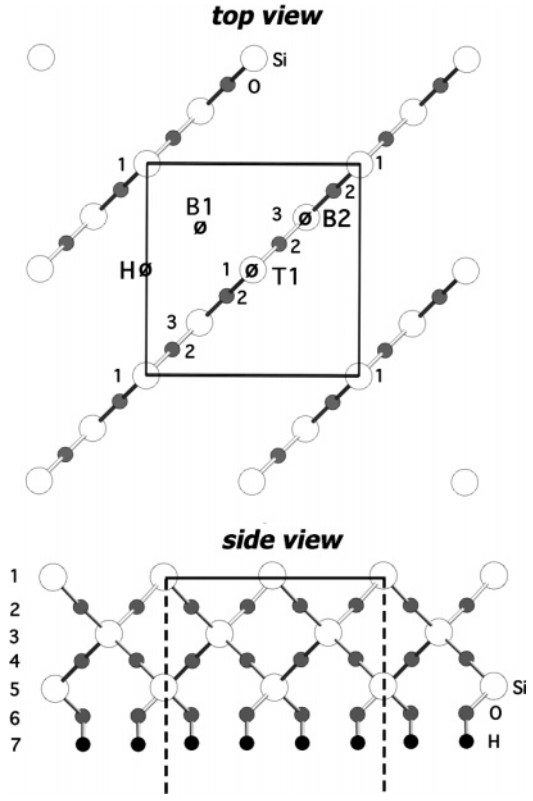

Figure 1. Top and side views of the β-cristobalite(100) slab model with a Si topmost layer. Different sites studied: bridge 1 (B1), bridge 2 (B2), top Si (T1), and hollow (H). The solid line shows the surface unit cell, and the numbers indicate the layer where the atoms are sited.

the two parallel frequencies, in both spin states. In T1 minimum, the O adatom is very far from the first Si layer ($z \approx 1.4-1.5$ Å), and the perpendicular movement approaches O to the Si atom in the direction of the strong SiO bond. The parallel movements are carried out along the lines T1−B2 and T1−B1 (Figure 1), where the interactions with the neighbor atoms (in the same or in the deeper layers) are clearly minor; therefore, the perpendicular frequency has to be the highest. However, in the B1 site the situation is almost the reverse; the O adatom is very close to the first Si layer ($z \approx -0.5$ to 0.2 Å), and now one of the parallel movements goes into the SiO bond direction (line B1−T1 in Figure 1), which implies a higher frequency, while the another parallel movement corresponds to a direction with less interaction (line B1−H in Figure 1), in a similar way as also occurs for the perpendicular movement.

The $d_{O_{ad}-Si}$ values for T1 and B1 minima (Table 3) are quite close to the bulk β-cristobalite values (Table 1). However, only a slight relaxation of the silica slab is produced in T1, but an

TABLE 3: Calculated DFT-GGA/PW91 Adsorption Energies and Geometries for Atomic Oxygen over the β-Cristobalite (100)−Si Six-Layer Slab Model on Different Sites[a]

								ν(cm^{-1})[d]		
site	spin	E_{exc} (eV)	E_{ad} (eV)	$d_{O_{ad}-Si}$ (Å)[b]	$d_{O_{ad}-O}$ (Å)[b]	$z_{O_{ad}}$ (Å)[c]	∠SiO$_{ad}$Si (deg)	⊥		||
T1	0	0	5.97	1.527	2.791	1.423	74.9	947.6	216.2	120.0
	1	2.79	3.18	1.526	2.802	1.526	73.7	951.6	231.3	145.7
H	1	0	0.16	3.531	3.298	0.406	167.6	221.3	98.1	157.1i
	0	0.60	−0.44	3.505	3.297	0.375	168.4	139.7	53.2	91.7i
B1	1	0	6.56	1.679	2.762	−0.541	142.4	374.5	816.6	270.1
	0	0.76	5.80	1.719	2.889	0.200	166.6	246.6	516.4	288.6
B2	1	0	0.44	2.815	2.682	1.145	132.5	178.3	131.2	166.0i
	0	0.46	-0.02	2.741	2.646	1.074	133.8	273.8	91.7	230.2i

[a] Captions defined in Table 2. Four layers are relaxed. [b] Distance between O adatom and the closest Si or the O atom. For hollow and bridge sites there are 2 or 4 equal distances (see Figure 1). [c] The z distance between for O adatom with respect the first layer. [d] Harmonic vibrational frequencies of the atomic adsorbate with respect to the rigid substrate.

important reconstruction is observed in B1. In this latter case, the Si−Si distance decreases from 5.196 Å (clean slab) to 3.416 Å (singlet state) or 3.179 Å (triplet state), and the d_{12} interlayer distance changes from 1.007 Å (clean slab) to 0.708 Å (singlet state) or 0.516 Å (triplet state).

The calculated adsorption energies for T1 and B1 sites (in this latter case its half value can be taken as the binding energy due to the formation of two SiO bonds) are slightly lower than the usual SiO bond dissociation enthalpies in the gas phase (e.g., 6.50 eV in SiO_2 or 8.29 eV in SiO at 25 °C[32]) or in β-cristobalite (e.g., 9.61 eV derived from its cohesive energy (Table 1)). Despite the absence of direct experimental adsorption (or desorption) energies for the present system,[38] the comparison with previous DFT studies for the O adsorption over several crystalline surfaces (e.g., E_{ad} equal to 2.0−2.5 eV on MgO-(001),[35] 3.5−5.0 eV on Pd or Ni(100),[25] or 4.2−6.4 eV on GaN-(0001)[39]) supports the magnitude of the chemisorption found. The differences observed in O−SiO_2 with O−MgO adsorption energies could be initially accounted for in terms of their different bond strengths. Thus, the bond dissociation enthalpies at 298 K for SiO and MgO gas-phase diatomic molecules are 8.29 and 3.50 eV,[32] respectively, which would be in agreement with the tendency observed in the O adsorption energies over β-cristobalite and periclase (MgO).[35] Moreover, the Mg and O surface atoms of periclase can compete simultaneously to adsorb the incoming O atom, while in β-cristobalite it is more difficult as Si and O atoms are distributed in different layers. In MgO (an ionic solid) it is observed that strongest bonds are formed with lattice O ions (e.g., E_{ad} = 1.43−2.04 eV for flat MgO (001)[35]) to form a peroxide ion (O_2^{2-}), whereas O is less adsorbed on Mg lattice ions (e.g., E_{ad} = 0.84 eV[35]) with a O_{ad}−Mg distance (ca. 2.0 Å) similar to the MgO distance in the bulk crystal (i.e., 2.109 Å) and with an O_{ad}−O distance within the range 1.55−2.27 Å (depending on the site). This is also in agreement with the higher bond dissociation enthalpy of O_2 (i.e., 5.16 eV at 298 K[32]). Therefore, in both cases (SiO_2 and MgO) the O adatom tries to be incorporated into the bulk (like a growing of the crystal), achieving similar geometrical and energy properties as in the lattice. In SiO_2 (a rather covalent solid) the O atom bonds to the Si dangling bonds, on top a Si (in T1 site) or forming a bridge (in B1 site), in such a way that neighboring silicon atoms share the O (oxygen bridging), in both cases with stronger (covalent) bonds than in MgO.

To understand better the differences observed in the chemical bonding for T1 and B1 sites in both electronic states, we have analyzed their α and β density of states (DOS) and their projected DOS onto the O adatom and the two underneath Si atoms of the first layer (labeled as Si_{1a} and Si_{1b}), which are involved in the bonding of these minima with different extent. Their plots are shown in Figure 3 along with the pDOS for free O atom and for the clean SiO_2 slab. In this latter case it is observed the existence of the Si dangling bond states (approximately in the −0.5 → 0 eV region). These electronic states are changed in the T1 (singlet) structure and appear now at more negative energies (approximately in the −4 → −2 eV region) due to their participation in a σ bonding with the O_{ad}. It is also observed their contribution to the σ * states at positive energies. Small shifts are observed for the DOS of both silicon atoms, with lower energies for the Si_{1a} states due to its major contribution to the bond. Moreover, as the total state is a singlet, a π bond can be established between O_{ad} and Si_{1a}, involving p_x or p_y orbitals (approximately in the −7 → −4 eV region). Thus, the O_{ad} passivates the two Si dangling bonds. Si_{1a} is also bonded to two oxygen atoms of the second layer with similar SiO

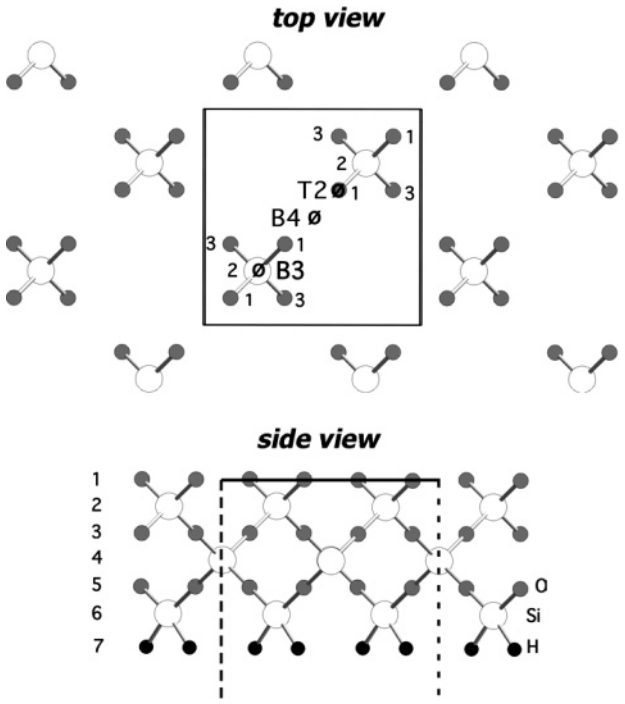

Figure 2. Top and side views of the β-cristobalite(100) slab model with an O topmost layer. Different sites studied: bridge 3 (B3), bridge 4 (B4), and top O (T2). The solid line shows the surface unit cell, and the numbers indicate the layer where the atoms are sited.

distances, keeping the four atoms in the same plane. For the T1 (triplet) structure, the O_{ad} projected DOS present a strong α polarization, which is also appreciated for Si_{1a} atom. On the contrary, Si_{2a} shows almost equal density of α and β states. Thus, this could be explained considering that both O_{ad} and Si_{1a} tend to keep one unpaired electron to produce the total triplet state. This fact would prevent the possibility to form a π SiO bond as it occurs in T1 (singlet) structure. Hence, this could justify the higher binding energy obtained for the singlet structure (E_{ad}(singlet) = 5.97 eV) compared with the triplet one (E_{ad}(triplet) = 3.18 eV). In T1 (singlet and triplet) structures the O_{ad} is quite above the first Si layer (z = 1.4−1.5 Å), and the deactivation of two Si_{1a} dangling bonds reduces the possibility of a significant relaxation of the slab. Thus, very similar geometries are obtained for both T1 structures (Table 3), and the slab changes are minor in comparison with the clean slab geometry.

In the B1 (singlet) structure, the adatom makes an oxygen bridging between two surface Si atoms. Thus, O_{ad} tends to become like an O of the slab. Their pDOS are very similar. Moreover, both Si atoms under the O_{ad} (i.e., Si_{1a} and Si_{1b}) present equivalent pDOS. The bonding between each Si and O_{ad} passivates one of the two initial Si dangling bonds, as can be shown in Figure 3 (shifted to the −6 → −5 eV region). The remaining Si dangling bond of each Si can react to form the reconstructed final structure as a consequence of the trend to bond pairing up, which is observed in semiconductor surfaces. This is also in agreement with the important reconstruction observed in both B1 structures, where in the final geometry the Si achieves a pyramidal structure (SiO_3), with Si very close to the surface (z = −0.5 to 0.2 Å). B1 structures (singlet and triplet) present similar binding energies (ca. 5.80/2 eV (singlet) and 6.56/2 eV (triplet)), which could be understood taking into account that now oxygen keeps two lone pairs and forms only a σ SiO bond with both Si atoms, regardless of the total spin of the system. The pDOS in B1 (triplet) structure indicate a spin

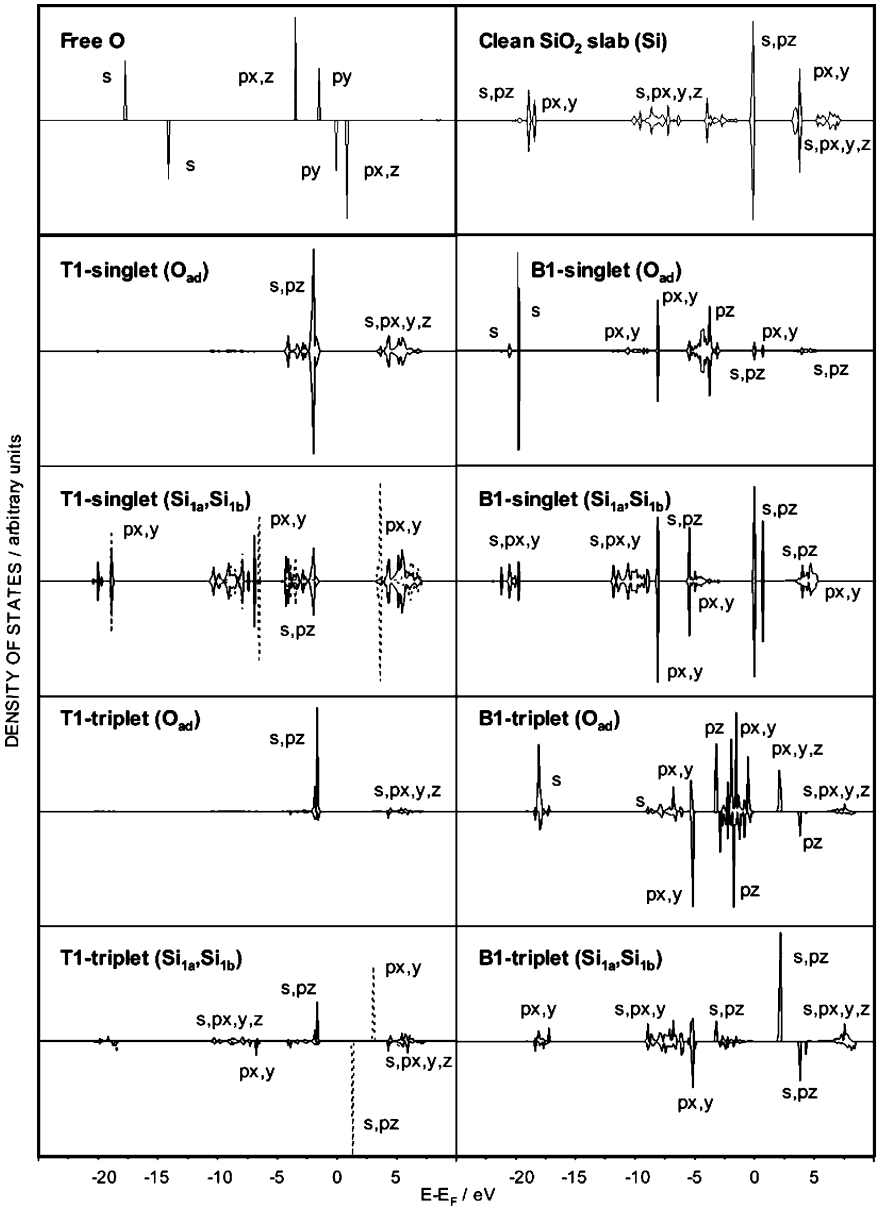

Figure 3. Density of states (DOS) projected onto surface silicon (two Si atoms in the first layer under O_{ad}) and oxygen adatom for T1 and B1 sites over β-cristobalite in both states (i.e., singlet and triplet). Both spin-up (top) and spin-down (bottom) portions are depicted. E_F indicates the Fermi energy. In T1 (singlet and triplet) plots, the solid lines are used for pDOS of the Si located right under the O_{ad} (labeled as Si_{1a}) and the dashed lines for the closest Si atom in the same layer (labeled as Si_{1b}). DOS for free oxygen and for surface Si atoms of β-cristobalite are also shown at the top of the figure. Some important peaks are labeled to facilitate de discussion presented in the text.

polarization due to O_{ad} and both Si atoms, which would mean some delocalization of two unpaired electrons.

The B2 and H structures correspond to very small adsorptions, mainly in the triplet state, even though these stationary points are not truly minima but transition states (i.e., first-order saddle points). In these structures there is no any significant geometrical relaxation with respect the clean slab geometry. We have also checked that the H structure seems to be a diffusion transition state that connects two equivalent B1 minima. Nevertheless, as surface reconstruction is important in B1 minimum, the analysis of the vibrational frequencies in H structure has to be taken as approximate due to the vibrational frequencies calculated, keeping fixed the slab geometry in both stationary points. In B2 structure this problem was not found, and it was much easier to establish that it corresponds to a diffusion transition state for the T1 interconversion.

The corresponding diffusion energy barriers are 5.99 eV (singlet state) and 2.74 eV (triplet state) for T1 → $B2^{\ddagger}$ → T1 and 6.24 eV (singlet state) and 6.40 eV (triplet state) for B1 → $H^{\ddagger}$ → B1. These high-energy barriers should be taken carefully as they imply two lateral migrations of the O adatom between equivalent sites that are quite distant each other. It can be expected than much lower barriers should exist for the interconversion between B1 and T1 minima; these structures are very close (along the T1−B1−T1 diagonal in surface cell shown in Figure 1) in geometry and energy; hence, another transition state (possibly located between T1 and B1 and involving some relaxation of the slab) with a lower energy barrier would allow an easier diffusion. This fact along with the possibility of another internal diffusions (not studied here) would be in better agreement with recent DFT values calculated for O diffusion inside α-quartz (i.e., 1.3 eV assuming a singlet state[21,40]) or to the O migration (diffusion) energy (i.e., 1. 65 eV) used in kinetic modeling of O and N recombination over silica reentry thermal protection systems.[5] However, for the study of O atomic collisions over silica the initial direct adsorption in B1 and T1

TABLE 4: Calculated DFT-GGA/PW91 Adsorption Energies and Geometries for Atomic Oxygen over the *Fdd*2 Derived *β*-Cristobalite (100)−Si Six-Layer Slab Model on Different Sites[a]

								ν (cm^{-1})[d]		
site	spin	E_{exc} (eV)	E_{ad} (eV)	$d_{O_{ad}-Si}$ (Å)	$d_{O_{ad}-O}$ (Å)	$z_{O_{ad}}$ (Å)	∠SiO$_{ad}$Si (deg)	⊥		||
T1	0	0	6.05	1.525	2.786	1.369	75.2	888.3	193.2	68.7
	1	2.77	3.28	1.526	2.795	1.526	72.9	952.2	196.9	77.3
H	1	0	0.21	3.469	3.003	0.364	168.5	117.3	103.7	88.8i
	0	0.58	−0.37	3.472	3.031	0.376	168.3	118.5	88.4	73.5i
B1	1	0	6.43	1.665	2.647	−0.389	152.7	343.4	882.8	313.3
	0	0.61	5.82	1.714	2.759	0.251	163.2	188.9	564.4	328.5
B2	1	0	0.54	2.684	2.668	1.117	130.8	192.9	70.5	236.7i
	0	0.38	0.16	2.562	2.579	0.936	137.1	218.0	118.3	323.9i

[a] Captions defined in Tables 2 and 3.

TABLE 5: Calculated DFT-GGA/PW91 Adsorption Energies and Geometries for Atomic Oxygen over *β*-Cristobalite (100)−O Six-Layer Slab Model on Different Sites[a]

								ν(cm^{-1})		
site	spin	E_{exc} (eV)	E_{ad} (eV)	$d_{O_{ad}-O}$ (Å)	$d_{O_{ad}-Si}$ (Å)	$z_{O_{ad}}$ (Å)	∠OO$_{ad}$O (deg)	⊥		||
T2	1	0	*b*	1.248	2.940	1.183	61.6			
	0	0.30	*b*	1.260	2.879	1.185	60.5			
B3	1	0	4.10	1.480	2.181	0.945	100.7	640.6	535.3	145.7i
	0	0.43	3.67	1.478	2.190	0.945	100.5	512.4	563.6	74.1
B4	1	0	3.38	1.484	3.129	0.513	139.5	547.7	136.7i	206.3i
	0	0.17	3.21	1.489	3.129	0.492	141.4	544.6	89.3i	217.2i

[a] Captions defined likewise as in Tables 2 and 3. Full relaxed slab model is considered. [b] Formation of an O_2 molecule occurs instead of the O adsorption process.

minima will be more relevant because the initial slight adsorption in H or B2 sites will evolve to the T1 and B1 minima.

In the previous section we discussed the bulk and slab models for clean *β*-cristobalite, and we proposed a slab model (relaxed) derived from a *Fd*3*m* bulk structure. To see the possible influence of the SiOSi angles of the slab in the O adsorption energies, we have also made calculations by using a slab model derived from a *Fdd*2 bulk structure (Table 1), which essentially means than the SiOSi angles are close to 147° instead of 180°. The results are presented in Table 4. The comparison with the results shown in Table 3 indicates that the adsorption energies and the geometries are very similar for all structures, and both slabs seem to be almost equivalent for the present study.

We have also studied the possible adsorption of oxygen on the *β*-cristobalite (100) face terminated with O atoms. Three several sites were finally considered: on top O (T2) and two bridges (B3 and B4), as shown in Figure 2. In this case we had to use the six-slab model with full relaxation to obtain converged results, which are shown in Table 5. In the first site (T2) we did not find an atomic adsorption but the abstraction reaction to produce the O_2 molecule without energy barrier. In both bridge sites a chemisorption was obtained either in the singlet or in the triplet state, with similar adsorption energies and very small geometrical relaxation in comparison with the clean slab geometry. The stability of both B3 structures (singlet and triplet) is coherent with the most stable Lewis structures, with two electron lone pairs in each O atom for the singlet B3 structure and with two unpaired electrons in two of the three oxygen atoms for the triplet.

The B4 stationary point is a diffusion transition state which connects two equivalent B3 (singlet) minima (i.e., for B3 → B4‡ → B3) with a small energy barrier ≤0.46 eV (singlet state). Nevertheless, B4 has two imaginary frequencies in both states, and it could be expected that a first-order saddle point should be close to the reported geometries. We have also calculated the vibrational frequencies for B4 structure (triplet state), relaxing the two first layers of the slab. All calculated frequencies were real except for two, which were associated with parallel movements of O adatom (183.7i, 356.9i). The perpendicular movement of the O adatom was approximately associated with a vibrational frequency of 373.5. These results are in agreement with the values reported in Table 5 (i.e., 547.7, 136.7i, 206.3i) and show that the existence of two imaginary frequencies is possibly due to the true transition state is slightly shifted from the reported geometry. Therefore, the rigid slab approximation for the vibrational frequency calculations seem to be appropriate enough to characterize the stationary points.

The number and the energy of the stationary points found points out that the Si face on *β*-cristobalite (100) will be more important than the O face for oxygen adsorption processes and probably also for the successive Eley−Rideal or Langmuir−Hinshelwood reactions, such as it has been assumed up to date in all kinetic modeling studies on air chemical processes over silica materials.[1]

3.3. Atomic Nitrogen Adsorption on *β*-Cristobalite. We have carried out a similar study as for oxygen using now atomic nitrogen. The same sites (Figures 1 and 2) were initially considered for this system in the two lowest spin states derived from the N(^{4}S) (i.e., doublet and quartet states). Table 6 summarizes the results for the *β*-cristobalite (100) with a first Si layer. First of all, it is not observed any adsorption (i.e., zero or negative E_{ad}) for H and B2 sites in whichever of both spin states. On the contrary, T1 and B1 sites correspond to important chemisorptions as it took also place for O adsorption, mostly in the doublet state. Both stationary points are really minima as the harmonic vibrational frequencies prove. Their d_{Nad-Si} values, shown in Table 6, are within the range of the usual N−Si distances in silicon nitrides in gas phase (e.g., 1.57 Å in SiN ($^2\Sigma^+$) or 1.70 Å in Si_2N ($^2\Pi_g$)[32]) or in nitride films on silicon (e.g., 1.62−1.76 Å[41]). Though a very small relaxation is observed for the slab in T1 site, there is a considerable reconstruction of the slab in the B1 site as it also happened for the O adsorption on the Si face. Thus, the Si−Si distance decreases from 5.196 Å (clean slab) to 3.256 Å (doublet state) or to 3.311 Å (quartet state), and the d_{12} interlayer distance

TABLE 6: Calculated DFT-GGA/PW91 Adsorption Energies and Geometries for Atomic Nitrogen over β-Cristobalite (100)−Si Six-Layer Slab Model on Different Sites[a]

								ν (cm^{-1})		
site	spin	E_{exc} (eV)	E_{ad} (eV)	$d_{N_{ad}-Si}$ (Å)	$d_{N_{ad}-O}$(Å)	$z_{N_{ad}}$ (Å)	∠SiN$_{ad}$Si (deg)	⊥		||
T1	1/2	0	2.88	1.649	2.886	1.538	73.7	804.8	241.8	191.9
	3/2	2.84	0.04	1.650	2.898	1.647	72.7	795.0	212.2	130.2
H	3/2	0	−0.05	3.404	3.211	0.193	174.1	292.5i	216.6	194.4
	1/2	1.21	−1.26	3.408	3.224	0.213	173.5	271.5i	200.9	193.8
B1	1/2	0	5.35	1.637	2.888	0.168	168.2	181.6	972.4	296.5
	3/2	1.80	3.55	1.775	2.792	−0.641	137.7	297.6	771.2	320.8
B2	3/2	0	−0.0004	3.151	3.103	1.752	112.4	226.7i	173.3	163.4
	1/2	1.08	−1.08	2.956	2.883	1.443	121.6	121.6	142.8	182.3i

[a] Captions defined likewise as in Tables 2 and 3.

TABLE 7: Calculated DFT-GGA/PW91 Adsorption Energies and Geometries for Atomic Nitrogen over β-Cristobalite (100)−O Six-Layer Slab Model on Different Sites[a]

								ν (cm^{-1})		
site	spin	E_{exc} (eV)	E_{ad} (eV)	$d_{N_{ad}-O}$ (Å)	$d_{N_{ad}-Si}$ (Å)	$z_{O_{ad}}$ (Å)	∠ON$_{ad}$O (deg)	⊥		||
T2	1/2	0	*b*	1.124	3.503	1.311	78.2			
	3/2	0.59	*b*	1.172	2.981	1.124	65.4			
B3	1/2	0	6.10	1.336	2.208	0.808	105.6	986.9	758.8	210.8
	3/2	0.44	5.66	1.442	2.158	1.032	100.9	915.9	607.2	310.9
B4	1/2	0	6.88	1.278	2.986	−0.099	105.3	941.4	880.2	125.2i
	3/2	1.40	5.48	1.380	2.986	0.374	100.8	739.9	573.5	118.3i

[a] Captions defined likewise as in Tables 2 and 3. Full relaxed slab model is considered. [b] Formation of a NO molecule occurs instead of the N adsorption process.

changes from 1.007 Å (clean slab) to 0.465 Å (doublet state) or 0.557 Å (quartet state).

The DFT adsorption energies for T1 and B1 sites are slightly lower than the typical Si−N bond dissociation enthalpies in the gas phase (e.g., 4.41 eV in Si_2N or 5.71 eV in SiN at 25 °C[32]). Although no direct experimental data are available for N adsorption on silica,[38] the present results compare reasonably well with earlier theoretical or experimental studies on the N adsorption over several solids (e.g., E_{ad} equal to 2.6−4.6 eV on Si(100), with similar values for doublet and quartet states,[41] or 3.35−5.65 eV on several Cu planes[42]). Moreover, a very recent cluster B3LYP-DFT study[43] on the N adsorption on Si_xO_y (silica clusters) reports an adsorption energy for the T1 site (i.e., 2.84 eV) and a N−Si distance (i.e., 1.7 Å) quite similar to our present values (Table 6), which is nonetheless based on periodic (slab) DFT-GGA/PW91 calculations.

The difference between doublet and quartet SiN binding energies in T1 structures (Table 6) could be justified in a similar way as it was made for O adsorption structures. Thus, the doublet state allows the possibility of a Si═N double bound as N can keep one unpaired electron; conversely, the quartet state makes even difficult the formation of a single bond due to the difficulty for N or Si (Si is also bonded to two O atoms of the slab) to have three unpaired electrons and simultaneously to make a bond, which is consistent with the unimportant bonding in quartet state for T1 structure. Similar arguments can be valid for B1 structures.

The stationary point corresponding to N adsorption in H site is a diffusion transition state that connects both equivalent B1 minima (i.e., B1 → H‡ → B1) with high energy barriers of 3.60 eV (doublet state) and 6.61 eV (quartet state). The B2 structure turns out to be a diffusion transition state connecting both equivalent T1 minima (i.e., T1 → B2‡ → T1) with energy barriers of 3.96 and 0.04 eV for doublet and quartet states, respectively. This behavior is similar as we observed for O adsorption and does not exclude the existence of even minor diffusion energy barriers for another directions (e.g., line T1−B1 in Figure 1).

The adsorption of N into the first oxygen face on the β-cristobalite (100) shows as well similar sites (Figure 2) and behavior as for O adsorption, and its results are indicated in Table 7. Thus, it is also observed a molecular formation (i.e., NO) in the T2 site for both spin states instead of the N adsorption process, with energy barrierless in both cases. Moreover, an important chemisorption is obtained in B3 site (true minimum) for both spin states. Their corresponding NO binding energies (6.10/2 eV and 5.66/2 eV in doublet and quartet states, respectively) are within the ordinary range of the NO bond dissociation enthalpies in gas phase (e.g., 3.18 eV in NO_2-($^2A_1$) or 6.55 eV in NO($^2\Pi$) at 25 °C [32]). The N_{ad}−O distances (1.336 and 1.442 Å in doublet and quartet states, respectively) are rather longer than the NO distances in small gas-phase molecules (e.g., 1.197 Å in NO_2($^2A_1$) or 1.151 Å in NO($^2\Pi$)[32]); only a very small slab relaxation is produced as in the case of O adsorption. In B3 minima, N is bonded to two oxygen atoms, which are also bonded to the same tetracoordinated Si atom (i.e., SiO_4 group in Figure 2). The slight difference in their binding energies (derived form E_{ad} values shown in Table 7) can be explained again, taking into account the major facility of the N atom to keep one unpaired electron (and a lone pair) when is also simultaneously making two NO bonds in the doublet state, which seems a bit more difficult for the quartet state.

The B4 stationary point corresponds to a diffusion transition state for the B3 interconversion (i.e., for B3 → B4‡ → B3), with a very small energy barrier of 0.18 eV for the quartet state. However, this transition state has a slightly lower energy than B3 minima for the doublet state; even though B3 minimum should be deeper than B4 transition state, the closeness of their energies could point out that B3 is a local minimum and the most stable one should be located not very far.

3.4. Atomic Sticking Coefficients and Desorption Rate Constants. The heat of chemisorption on a polycrystalline surface represents an average of the binding energies of the different surface sites weighted according to the relative concentrations of these sites. In a single-crystal surface as the

TABLE 8: Calculated DFT-GGA/PW91 O and N Average Adsorption Energies on the β-Cristobalite (100)

first layer	E_{ad-O} (eV)[a]	E_{ad-N} (eV)[a]
Si	5.89	4.12
	4.87	1.80
O	4.10	6.10
	3.67	5.66

[a] The two values correspond to the singlet and triplet states for O and to the doublet or quartet states for N.

β-cristobalite (100), either terminated with Si or O, we can also estimate an average adsorption energy taking into account the active site concentration of a completely free surface (i.e., n_s^0 will be the number of true adsorption minima by surface cell area), assuming the same initial sticking coefficient for these sites and a small effect of the coverage on the adsorption energies as we have checked using some 2×2 surface cell calculations. Thus, n_s^0 becomes equal to 3.6×10^{18} sites/m^2 for T1, B1, or B3 sites (see Figures 1 and 2), and the average adsorption energies for O and N adsorption on the Si (or O) first face of β-cristobalite (100) are compared in Table 8. These values can easily be corrected for vibrational zero point energy using the harmonic vibrational frequencies shown in the previous tables, although the effect will be very small (i.e., a reduction less than 0.1 eV in the E_{ad}). These results show that O adsorption is preferred on the Si face of β-cristobalite (100) in comparison with the O face and that the reverse behavior is observed for N adsorption. On the other hand, the stronger chemisorption of O over β-cristobalite (100) than for N in the Si face is in total agreement with the usual assumption (see Introduction) made in kinetic modeling for hypersonic reactive air flows over silica materials.[1] A study in progress about the adsorption over the (111) first Si face of β-cristobalite shows similar conclusions as for the (100) face (e.g., $E_{ad-O} = 5.45$ eV (singlet) or 2.72 eV (triplet), and $E_{ad-N} = 3.08$ eV (doublet) or 1.00 eV (quartet), for an equivalent T1 site). Thus, these results could also suggest that the existence of terraces, steps, or corners on silica would not give much higher adsorption energies than on the flat β-cristobalite (100) surface.

To see the influence of these adsorption/desorption energies on the aforementioned kinetic models, we have also calculated the atomic initial sticking coefficients ($S_{0(A)}$) and desorption rate constants ($k_{des(A)}$) by means of the standard transition state theory (TST)[44] expressions used in this kind of studies[1,6] for nonactivated adsorptions and thermal equilibrium between the colliding A atoms and the wall (i.e., $T_g = T_W = T$):

$$S_{0(A)}(T) = \frac{n_S^0 h^2}{2\pi m_A k_B T} \prod_{i=1}^{2} \left[\frac{e^{-\nu_{||,i} h/2k_B T}}{1 - e^{-\nu_{||,i} h/k_B T}} \right] \quad (2)$$

and

$$k_{des(A)}(T) = \frac{k_B T}{h} e^{-E_{ads(A)}/RT} \left[\frac{1 - e^{-\nu_\perp h/k_B T}}{e^{-\nu_\perp h/2k_B T}} \right] \quad (3)$$

where m_A is the A atom mass, $\nu_{||}$ and $\nu_\perp$ are the two parallel and one perpendicular vibrational frequencies of the adatom A, respectively, and the rest of symbols have their usual meanings. In both equations we do not introduce the catchall factor (i.e., $P_{des} = 1$), which often is taken as an adjustable parameter in some kinetic models.[1]

Figure 4 illustrates the calculated initial sticking coefficients for O and N over a first Si face of β-cristobalite (100) against the temperature taking into account both minima (B1 and T1).

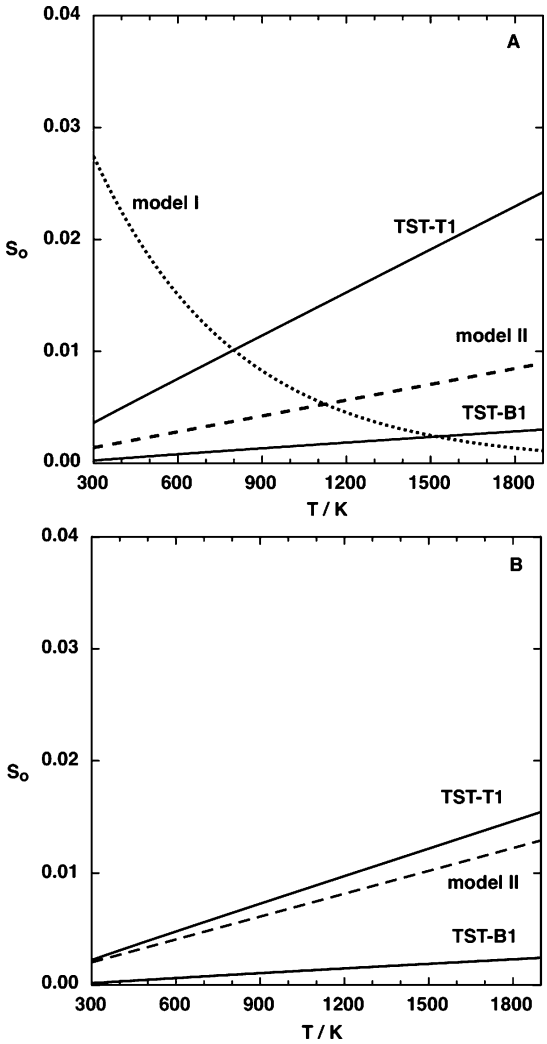

Figure 4. Initial sticking coefficients for O (A) and N (B) on silica: TST-site B1, TST-site T1, model I (ref 3), and model II (ref 6). TST curves are calculated for β-cristobalite (100) Si face by using eq 2 and the most stable adsorption minima.

The current DFT-TST results correspond to the ground electronic state in both systems (i.e., highest adsorption energies). The results of two empirical kinetic models (model I[3] and model II[6]) are also added for comparison. Model I takes into account the O adsorption, the O thermal desorption, and the O_2 formation by recombination of atomic oxygen (ER mechanism) by means of the corresponding time-dependent rate equations and using the following empirical expressions for S_0(A) and k_{des}(A):

$$S_{0(A)}(T) = Be^{-CT} \quad (4)$$

$$k_{des(A)}(T) = \frac{k_B T}{h} e^{-E_{ad(A)}/RT} \quad (5)$$

Thus, several physiochemical parameters were checked or optimized (i.e., $n_s^0 = 5 \times 10^{18}$ sites/m^2, $B = 0.05$, $C = 0.002$ K^{-1}, $E_{ad} = 3.5$ eV, and the activation energy (1 kcal/mol) and the steric factor (0.1 at $T \geq 925$ K) for the ER reaction) to match the experimental $\gamma_O(T)$ curve for O over silica in the range 20−600 °C; the authors also presented extrapolations of their results for higher temperatures (i.e., $T \leq 2000$ K). Model II distinguishes adsorption, desorption, recombination reactions (ER and LH mechanisms), and dissociative adsorption for N/N_2 and O/O_2 systems on silica. Transition state theory (e.g., eqs 2

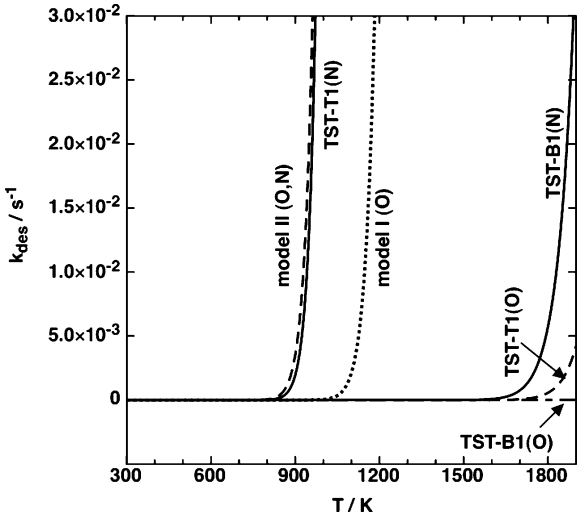

Figure 5. Desorption rate constants for O and N on silica: model I (ref 3), model II (ref 6), and TST-site B1 and TST-site T1 results for both O and N adsorption. TST curves are calculated for β-cristobalite (100) Si face by using eq 3 and the most stable adsorption minima.

and 3) and collision theory were used to derive the corresponding rate equations and a final expression of $\gamma_A(T)$. Some parameters were assumed (e.g., $n_s^0 = 2 \times 10^{18}$ sites/m^2, $E_{ad} =$ 2. 6 eV for N or O, $\nu_{||} = 62.6$ cm^{-1} for O and 55.6 cm^{-1} for N, $\nu_{\perp} = 417.0$ cm^{-1} for O or N, etc.), and others were adjusted to reproduce better the experimental $\gamma_O(T)$ and $\gamma_N(T)$ data (e.g., activation energies for ER and LH reactions, some steric factors, etc.); the authors also extrapolated their results until 2500 K.

Our calculated TST values agree with the low S_0 values derived in both kinetic models. Moreover, its temperature dependence is much closer to the model II shape, which is in between T1 and B1 curves for both systems.

In Figure 5 we show the calculated desorption rate constants for O and N over a first Si face of β-cristobalite (100) in front of the temperature for B1 and T1 minima. They are compared with the curves derived from both empirical models; in model I[3] it is assumed a value of 3.5 eV for the O adsorption energy, and in model II[6] it is taken as the same adsorption energy for O and N (2.6 eV), although the use of a factor in eq 3 (i.e., $P_{des} = 0.1$). The differences observed in the desorption rate constants are mainly produced because of the different DFT adsorption energies. Thus, there is better agreement for N adsorption, where our calculated adsorption energy for T1 site is close to those used in models I and II, but there are important differences for oxygen adsorption as we obtain much higher adsorption energies in both T1 and B1 sites. Therefore, our results show a clear different behavior for N and O. Nevertheless, as we pointed out in the Introduction, there is a broad range of E_{ad} derived from kinetic modeling on O and N recombination on silica-based surfaces. Thus, for instance, values such high as 5.95 eV have been used in another kinetic models for O and N recombination over RCG surfaces,[45] which would be much closer to our current DFT results.

These high adsorption energies imply that the chemisorbed atoms will be desorbed only at relatively high temperatures ($T >$ 900 K for N and $T >$ 1800 K for O from Figure 5), so that these atoms will be held irreversibly on the surface and they will be removed only by atomic recombination (e.g., ER or LH processes) at lower temperatures. Experimental studies by using single-crystal adsorption calorimeter[38,46] or thermal desorption spectroscopy[46] would be necessary to validate entirely our theoretical results. The calculated $S_{0(A)}$ and $k_{des(A)}$ for N and O would tend to increase the corresponding γ_A coefficients if the kinetic data[6] for ER and LH were kept constant. However, a DFT study on the minimum-energy paths and the transition states involved in ER and LH reactions (in progress in our group) will be necessary to obtain an accurate calculation of $\gamma_A(T)$ coefficients.

Finally, despite the assumptions made in the $S_{0(A)}$ and $k_{des(A)}$ calculations—TST equations, single crystal, Si face, small effect of the coverage in DFT adsorption energies, etc.—we believe that our values are more suitable to be used in the mentioned kinetic models than the usual adjustable (semiempirical) parameters not derived from first principles, which differ considerably among the numerous empirical kinetic studies made up to date.

4. Summary and Conclusions

In this work we have made a periodic DFT study (GGA/PW91) on the adsorption of atomic oxygen and nitrogen over β-cristobalite (100) considering the two lowest spin states of every system and the termination of the crystalline SiO_2 with a first face of Si or O.

Bulk calculations on different spatial symmetries of β-cristobalite show a good agreement with experimental and previous theoretical data, which gives additional reliability to the DFT method used in the work. Moreover, the slab model chosen to simulate the β-cristobalite (i.e., 6 layers relaxing 4 or 6) reproduces the main geometrical properties of experimental β-cristobalite and shows a good convergence on the adsorption properties for O and N.

The adsorption of O over β-cristobalite (100) indicates a strong chemisorption in two sites (on top Si and in a bridge) for a first Si layer, with an average adsorption energy of 5.89 eV (singlet state) or 4.87 eV (triplet state). For a slab terminated with an O layer the adsorption energy (bridge 3) is 4.10 eV (singlet state) or 3.67 eV (triplet state). The adsorption of N presents similar results. Thus, for a first Si layer we obtain an average adsorption energy of 4.12 eV (doublet state) or 1.80 eV (quartet state). For a slab ended with an O layer the adsorption energy in bridge 3 is 6.10 eV (doublet state) or 5.66 eV (quartet state). The values of the different adsorption energies, which depend on the adatom, the site, and the spin state involved, can be qualitatively explained by analyzing the kind of bonds formed in each case.

The approach of either O or N on top oxygen of β-cristobalite (100) gives place to the abstraction reactions, which produce O_2 or NO molecules, respectively, without energy barrier.

Several diffusion transition states have also been characterized, which connect some of the adsorption minima with rather high energy barriers; this does not exclude the existence of much lower energy barriers in another directions of the cell (e.g., in the line between B1 and T1 minima).

Atomic sticking coefficients and desorption rate constants have been estimated within the temperature range 300−1900 K by means of the usual transition state equations and the standard approximations. The high adsorption energies found for O and N over silica imply that the atomic recombination processes (i.e., Eley−Rideal and Langmuir−Hinshelwood mechanisms) will have a more important role in the atomic detachment processes than the thermal desorption processes at temperatures lower than 1800 K for O and 900 K for N. Further experimental data should confirm these conclusions along with DFT calculations on these reactions, in progress in our research group.

Finally, the magnitude of the DFT adsorption energies also suggests that the published kinetic models of atomic O and N recombination on SiO_2 surfaces, which make use of low adsorption energies (e.g., 3.5 eV equal for O and N[1]), should be revised, particularly for oxygen processes. It can be expected that the structural differences in silica based-materials (e.g., Pyrex, cristobalite, RCG, etc.) will not give a large divergence in adsorption energies and hence that the present values could be still suitable for them.

Acknowledgment. We thank Prof. A. Salin and H. F. Busnengo for useful discussions in the final part of this work and Prof. M. Cacciatore for sending us a copy of ref 43. This work has been supported by the "Dirección General de Enseñanza Superior (Programa Sectorial de Promoción General del Conocimiento)" of the Spanish Ministry of Science and Technology (DGES Project ref BQU2002-03351). The authors are grateful to the "Centre de Supercomputació de Catalunya (CESCA)" for providing a part of the computer time.

References and Notes

(1) Capitelli, M., Ed.; *Molecular Physics and Hypersonic Flows*; NATO ASI Series C, Vol. 482; Kluwer Academic Publishers: Dordrecht, 1989.
(2) Kurotaki, T. AIAA paper 2000−2366, 2000.
(3) Seward, W. A.; Jumper, E. J. *J. Therm. Heat Trans.* **1991**, *5*, 284.
(4) Jumper, E. J.; Seward, W. A. *J. Therm. Heat Trans.* **1994**, *8*, 460.
(5) Nasuti, F.; Barbato, M.; Bruno, C. *J. Therm. Heat Trans.* **1996**, *10*, 131.
(6) Daiss, A.; Frühauf, H.-H.; Messerschmid, E. W. *J. Therm. Heat Trans.* **1997**, *11*, 346.
(7) Balat, M. J. H.; Czerniak, M.; Badie, J. M. J. *Space Rock.* **1999**, *36*, 273.
(8) Balat-Pichelin, M.; Badie, J. M.; Berjoan, R.; Boubert, P. *Chem. Phys.* **2003**, *291*, 181.
(9) Cacciatore, M.; Rutigliano, M.; Billing, G. D. *J. Therm. Heat Trans.* **1999**, *13*, 195.
(10) Kresse, G.; Hafner, J. *Phys. Rev. B* **1993**, *48*, 13115.
(11) Kresse, G.; Hafner, J. *Phys. Rev. B* **1994**, *49*, 14251.
(12) Kresse, G.; Furthmüller, J. *Comput. Mater. Sci.* **1996**, *6*, 15.
(13) Kresse, G.; Furthmüller, J. *Phys. Rev. B* **1996**, *54*, 11196.
(14) Perdew, J. P.; Chevary, J. A.; Vosko, S. H.; Jackson, K. A.; Pederson, M. R.; Singh, D. J.; Fiolhais, C. *Phys. Rev. B* **1992**, *46*, 6671.
(15) Perdew, J. P.; Wang, Y. *Phys. Rev. B* **1992**, *45*, 13244.
(16) Blöchl, P. E. *Phys. Rev. B* **1994**, *50*, 17593.
(17) Kresse, G.; Joubert, D. *Phys. Rev. B* **1999**, *59*, 1758.
(18) Monkhorst, H. J.; Pack, J. D. *Phys. Rev. B* **1976**, *13*, 5188.
(19) Ma, Q.; Klier, K.; Cheng, H.; Mitchell, J. W.; Hayes, K. S. *J. Phys. Chem. B* **2000**, *104*, 10618.
(20) Baraille, I.; Loudet, M.; Lacombe, S.; Cardy, H.; Pisani, C. *J. Mol. Struct. (THEOCHEM)* **2003**, *620*, 291.
(21) Akiyama, T.; Kageshima, H. *Appl. Surf. Sci.* **2003**, *216*, 270.
(22) Seminario, J. M., Ed.; *Recent Advances and Applications of Modern Functional Theory, Theoretical and Computational Chemistry*; Elsevier Science: Amsterdam, 1996; Vol. 4, Chapter of A. Savin *On degeneracy, near-degeneracy and density functional theory*, p 327.
(23) Baerends, E. J.; Branchadell, V.; Sodupe, M. *Chem. Phys. Lett.* **1997**, *265*, 481.
(24) Perdew, J. P.; Burke, K.; Ernzerhof, M. *Phys. Rev. Lett.* **1996**, *77*, 3865.
(25) Hammer, B.; Hansen, L. B.; Nørskov, J. K. *Phys. Rev. B* **1999**, *59*, 7413.
(26) Wyckoff, R. W. G. *Crystal Structures*; John Wiley & Sons: New York, 1963; Vol. 1.
(27) Barth, T. F. W. *Am. J. Sci.* **1932**, *23*, 350.
(28) Wright, A. F.; Leadbeter, A. J. *Philos. Mag.* **1975**, *31*, 1391.
(29) Keeffe, M. O.; Hyde, B. G. *Acta Crystallogr.* **1976**, *B32*, 2923.
(30) Demuth, Th.; Jeanvoine, Y.; Hafner, J.; Ángyán, J. G. *J. Phys.: Condens. Matter* **1999**, *11*, 3833.
(31) Liu, F.; Garofalini, S. H.; King-Smith, R. D.; Vanderbilt, D. *Phys. Rev. Lett.* **1993**, *70*, 2750.
(32) Chase, M. W., Jr.; Davies, C. A.; Downey, J. R., Jr.; Frurip, D. J.; McDonald, R. A.; Syverud, A. N. *J. Phys. Chem. Ref. Data* **1985**, *14*, Suppl. 1.
(33) Liu, F.; Garofalini, S. H.; King-Smith, D.; Vanderbilt, D. *Phys. Rev. B* **1994**, *49*, 12528.
(34) Song, S.; VanGinhoven, R. M.; Corrales, L. R.; Jónsson, H. *Faraday Discuss.* **2000**, *117*, 303.
(35) Kantorovich, L. N.; Gillan, M. J. *Surf. Sci.* **1997**, *374*, 373.
(36) Jacob, T.; Muller, R. P.; Goddard III, W. A. *J. Phys. Chem. B* **2003**, *107*, 9465.
(37) Jacob, T.; Merinov, B. V.; Goddard III, W. A. *Chem. Phys. Lett.* **2004**, *385*, 374.
(38) Brown, W. A.; Kose, R.; King, D. A. *Chem. Rev.* **1998**, *98*, 797.
(39) Naia-Xia, L.; Jun-Qian, L.; Yi-Jun, X.; Wen-Kai, C.; Yong-Fan, Z. *J. Mol. Struct. (THEOCHEM)* **2004**, *668*, 51.
(40) Hamann, D. R. *Phys. Rev. Lett.* **1998**, *81*, 3447.
(41) Widjaja, Y.; Heyman, A.; Musgrave, C. B. *J. Phys. Chem. B* **2002**, *106*, 2643.
(42) Zhao-Yu, D.; Xiao-Ming, Z.; Ze-Xin, W.; Ling-Li, H. *Chin. J. Chem.* **2004**, *22*, 1225.
(43) Laganá A., Gavrilova M. L., Kumar, V., et al., Eds.; *Lecture Notes in Computer Science, Computational Science and Its Applications−ICCSA 2004;* Springer-Verlag: Heidelberg, 2004; Vol. 3044, Chapter of Cacciatore, M., Pieretti, A., Rutigliano, M., Sanna, N., *From DFT cluster calculations to molecular dynamics simulation of N2 formation on a silica model surface*, p 366.
(44) Wilkinson, F. *Chemical Kinetics and Reaction Mechanisms*; Van Nostrand Reinhold Co.: Norfolk, 1981.
(45) Willey, J. *J. Therm. Heat Trans.* **1993**, *7*, 55.
(46) Cerny, S. *Surf. Sci. Rep.* **1996**, *26*, 1.